Available online at www.sciencedirect.com
ScienceDirect
Journal of Hazardous Materials 158 (2008) 517–522
Journal of Hazardous Materials
www.elsevier.com/locate/jhazmat

Preparation and photoelectrocatalytic activity of ZnO nanorods embedded in highly ordered TiO_2 nanotube arrays electrode for azo dye degradation

Zhonghai Zhang, Yuan Yuan, Linhong Liang, Yuxiao Cheng, Guoyue Shi, Litong Jin *

Department of Chemistry, East China Normal University, Shanghai 200062, China

Received 14 November 2007; received in revised form 2 January 2008; accepted 29 January 2008
Available online 10 March 2008

Abstract

In this article, the ZnO nanorods embedded in highly ordered TiO_2 nanotube arrays (ZnO/TiO_2 NR/Ts) electrodes were fabricated through two steps: (1) electrosynthesis of TiO_2 nanotube arrays (TiO_2 NTs) in HF solution by anodization method; (2) followed by cathodic electrodeposition of ZnO embedded in the TiO_2 nanotube arrays. The morphological characteristics and structures of ZnO/TiO_2 NR/Ts electrodes were examined by field-emission scanning electron microscopy (FE-SEM), energy dispersive X-ray (EDX) spectroscopy, X-ray diffraction (XRD) analysis, and UV–vis spectra. The linear-sweep photovoltammetry response on the ZnO/TiO_2 NR/Ts electrode was presented and the photocurrent was dramatically enhanced on the ZnO/TiO_2 NR/Ts electrode, comparing with that on bare TiO_2 NTs electrode. The photocatalytic and photoelectrocatalytic activity of ZnO/TiO_2 NR/Ts electrode was evaluated in degradation of methyl orange (MO) in aqueous solution.

Keywords: TiO_2 nanotubes; ZnO nanorods; Photoelectrocatalytic; Photocatalytic; Methyl orange

1. Introduction

Since Fujishima and Honda found a TiO_2 anode could split water into H_2 and O_2 under UV irradiation [1], enormous efforts have been devoted to the research of TiO_2 nanomaterials [2–16]. Recently, the research of vertically oriented, highly ordered TiO_2 nanotube arrays (TiO_2 NTs) was becoming of importance in a variety of fields, such as fabrication of dye-sensitized solar cells (DSCCs) and environmental protection, and received considerable attention [17–27]. The aligned uniform nanotube structure dramatically improved charge transport properties, which greatly contributed to the superior photoelectrochemical performance.

As another promising heterogeneous photocatalyst, semiconductor ZnO has also been intensively investigated for environmental remediation or photovoltaic devices [28–32]. The modification of the TiO_2 nanomaterials with other semiconductors could alter the charge transfer properties between TiO_2 and the surrounding environment [33]. In this study, the ZnO was cathodic deposited inside the TiO_2 nanotube channels to fabricate the ZnO nanorods embedded TiO_2 nanotubes (ZnO/TiO_2 NR/Ts) hybrid nanomaterials. In this process, the ZnO was used as photoelectrochemical modifying reagent. The photoelectrochemical performance was significantly enhanced on the ZnO/TiO_2 NR/Ts electrode compared that on pure TiO_2 NTs. The semiconductor energy band theory can be used to explain the photoelectrochemical mechanism of ZnO/TiO_2 NR/Ts. As the ZnO/TiO_2 NR/Ts absorb the UV light, a great number of electrons are promoted from the valence band (VB) to the conduction band (CB) of ZnO and TiO_2, leading to the generation of electron/hole (e^-/h^+) pairs. Though the ZnO possesses an energy band similar to that of TiO_2, it still plays an important role in electron transport. The electrons transfer from the CB of ZnO to the CB of TiO_2, and conversely, the holes transfer from the VB of TiO_2 to the VB of ZnO, that give rise to decrease of the pairs' recombination rate. The charge transport in the ZnO/TiO_2 NR/Ts is no doubt a key step for increasing the photoelectrochemical performance. The formation of photocurrent is due

* Corresponding author. Tel.: +86 21 62232627; fax: +86 21 62232627.
E-mail address: ltjin@chem.ecnu.edu.cn (L. Jin).

0304-3894/$ – see front matter © 2008 Published by Elsevier B.V.
doi:10.1016/j.jhazmat.2008.01.118

to the photogenerated electrons driven by the applied positive potential to the counter electrode. ZnO can increase the concentration of free electrons on the CB of TiO_2; this result implies that the charge recombination reduces in the process of electron transport. All the above results increase the availability of the photogenerated holes on the surface of the ZnO/TiO_2 NR/Ts and consequently an improvement of the photoelectrochemical performance can be expected.

In the present work, we used ZnO/TiO_2 NR/Ts electrodes to study the photocatalytic and photoelectrocatalytic degradation of azo dye, such as methyl orange (MO). MO is selected as a model dyeing pollutant because it is one of the most important commercial dyes, has a very short excited-state lifetime, and is stable to visible and near UV light [34]. The TiO_2 NTs, in this study, were used not only as photocatalytic semiconductor materials but also as template, which provided a general way to prepare novel hybrid nanomaterials.

2. Experimental details

2.1. Materials

Pieces of titanium sheets (purity > 99.7% and dimension: 15 mm × 7 mm × 0.5 mm) were purchased from Tite Inc., Shanghai. Zinc nitrate, hydrofluoric acid, sodium sulfate, methyl orange, and ethanol were of analytical grade from Shanghai Chemical Reagent Company (China) without further purification. All solutions were prepared with doubly distilled deionized water.

2.2. Preparation of ZnO/TiO_2 NR/Ts

Two processes were applied to the preparation of ZnO/TiO_2 NR/Ts

Process A: The electrochemical anodic oxidation technique was used to fabricate the TiO_2 NTs. Prior to anodization, the Ti sheets were first mechanically polished with different abrasive papers and rinsed in an ultrasonic bath of cold distilled water for 10 min. Then the cleaned Ti sheets were soaked in a mixture of HF and HNO_3 acids for 1 min (the mixing ratio of HF:HNO_3:H_2O is 1:4:5 in volume). After rinsed with acetone and deionized water for 10 min, the Ti sheets were dried in air at room temperature. The TiO_2 NTs were fabricated in a cylindrical electrochemical reactor (the radius is 30 mm and height is about 70 mm). 0.5 wt% hydrofluoric acid was used as the electrolyte and a platinum electrode served as the cathode during the entire process. A potential of 20 V was used and anodization time of 20 min was spent in this study. Anodized Ti sheets were annealed in dry oxygen environment at 500 °C for 1 h; heating and cooling rates were kept at 2.5 °C min^{-1}. The high density, well ordered and uniform TiO_2 nanotubes array was fabricated.

Process B: Direct cathodic electrodeposition of ZnO nanorods was performed in the TiO_2 NTs. The TiO_2 NTs served as the working electrode in a conventional three-electrode system, and a saturated calomel electrode (SCE) and a platinum electrode served as the reference and counter electrode, respectively. The electrolyte was prepared by dissolving 1 mM $Zn(NO_3)_2$ in deionized water. The cathodic potentials were used at −1.0 V with deposition times ranging from 20 to 60 min at 350 K. The electrochemical deposition reactions to prepare ZnO nanorods are proposed as follows:

$$Zn(NO_3)_2 \rightarrow Zn^{2+} + 2NO_3^- \quad (1)$$

$$NO_3^- + H_2O + 2e^- \rightarrow NO_2^- + 2OH^- \quad (2)$$

$$Zn^{2+}2OH^- \rightarrow Zn(OH)_2 \quad (3)$$

$$Zn(OH)_2 \rightarrow ZnO + H_2O \quad (4)$$

After that, the ZnO nanorods were embedded into the TiO_2 nanotubes (ZnO/TiO_2 NR/Ts).

2.3. Characterization of ZnO/TiO_2 NR/Ts

For verification of the formation of ZnO/TiO2 NR/Ts, the field-emission scanning electron microscopy (FE-SEM, Hitachi S-4800) under the voltage of 15 kV, energy dispersive X-ray (EDX Genesis fitted to the Hitachi FE-SEM S4800) analysis, X-ray diffraction (XRD, Model D/max 2550 V, Rigaku Co., Japan) analysis, and UV–vis absorption spectrum measurements (Varian Model Cary 50) were performed with $BaSO_4$ as a reflectance standard in this experiment [35].

2.4. Photoelectrochemical experiments

All photoelectrochemical measurements and photoelectrocatalytic application were conducted in a single photoreactor, as shown in Fig. 1. The ZnO/TiO_2 NR/Ts electrode with an active area of 1.0 cm^2 was placed in the photoreactor as the working electrode, and a SCE and a platinum electrode served as the reference and counter electrode, respectively. All the potentials were referred to SCE unless otherwise stated in this paper. Photocurrent and photopotential were measured using a CH Instruments 1232 electrochemical workstation (CH Instruments Inc., USA). An 11 W UV lamp with central wavelength of 253.7 nm and maximal light intensity of 10 mW/cm^2 was used as light source to measure the degradation efficiency of photoelectrocatalytic degradation of MO. A 0.5 M Na_2SO_4 aqueous solution (pH 6.2) was used as supporting electrolyte. MO aqueous solution (5×10^{-5} M) was used in the photoelectrocatalytic reaction and the pH value of the solution was not controlled during the reactive process.

2.5. Analytical methods

The UV–vis absorbance of MO solution showed two maxima: the first one was observed at 270 nm and the second one, more intensive, was observed at 470 nm. There existed an excellent linear relationship between the absorbance at 470 nm and the concentration of MO solution. The chemical oxygen demand (COD) values, whose decrease represented the removal

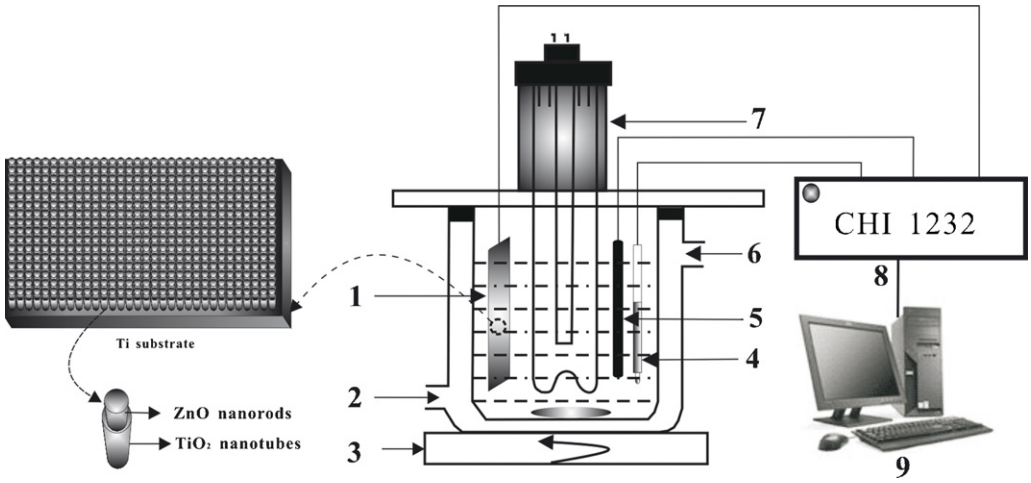

Fig. 1. Schematic diagram of photoelectrochemical reactor. (1) ZnO/TiO_2 NR/Ts electrode; (2) inlet of cooling water; (3) magnetic stirrer; (4) stirrer; (5) reference electrode; (6) counter electrode; (7) outlet of cooling water; (8) UV lamp; (9) electrochemical workstation; (10) computer.

of organic compounds, were estimated by COD standard method [36].

3. Results and discussion

3.1. SEM images and EDX analysis of ZnO/TiO_2 NR/Ts electrode

The SEM image of the TiO_2 NTs formed on the Ti substrate by anodization method is shown in Fig. 2a, which reveals that high density, well ordered and uniform nanotube arrays are formed. The diameters of these nanotubes range from 30 to 90 nm, with wall thicknesses of approximately 10 nm and their lengths range from 200 to 300 nm. After 20 min of ZnO cathodic deposition on TiO_2 NTs, as shown in Fig. 2b, the ZnO grows oriented through the TiO_2 nanotube inner channels, which describes the growing intergradation of ZnO nanorods. Fig. 2c shows the ZnO/TiO_2 NR/Ts SEM image after 60 min of cathodic deposition, the epitaxial growth of oriented ZnO nanorods inside the TiO_2 nanotube channels are formed and spilled over the TiO_2 NTs. The lengths of ZnO nanorods are about 100–200 nm outer the TiO_2 nanotube channels. The EDX analysis is carried out to identify the elemental composition of ZnO/TiO_2 NR/Ts, and the EDX spectrum has been shown in Fig. 2d, which shows strong

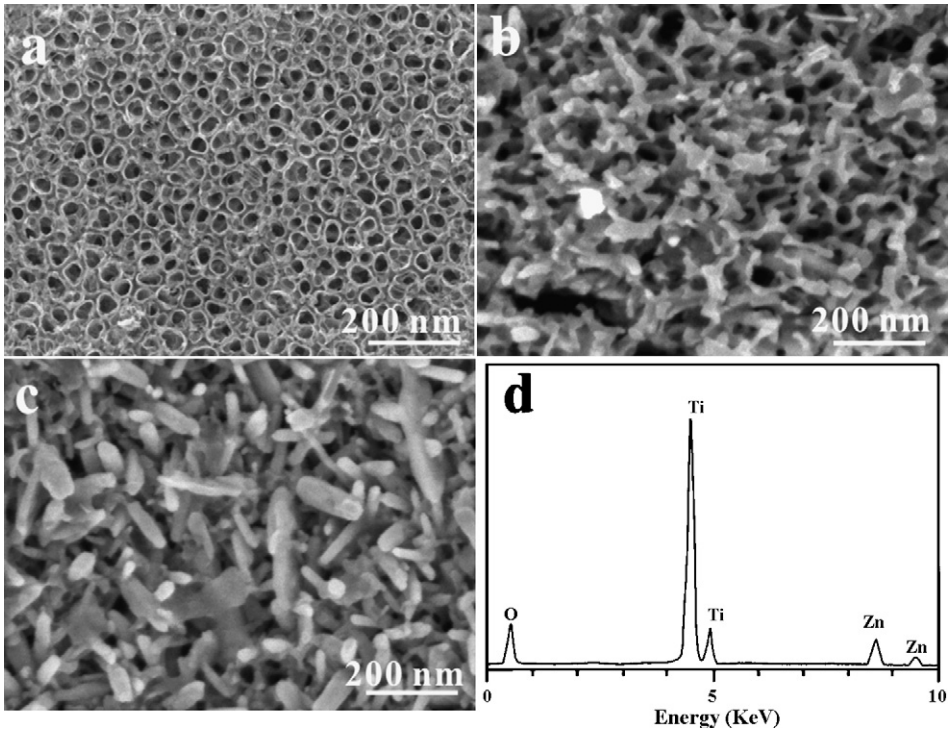

Fig. 2. (a) Top-view SEM image of TiO_2 NTs. (b and c) Top-view SEM images of ZnO cathodic deposition on TiO_2 NTs substrate for 20 and 60 min, respectively. (d) EDX spectrum of ZnO/TiO_2 NR/Ts sample.

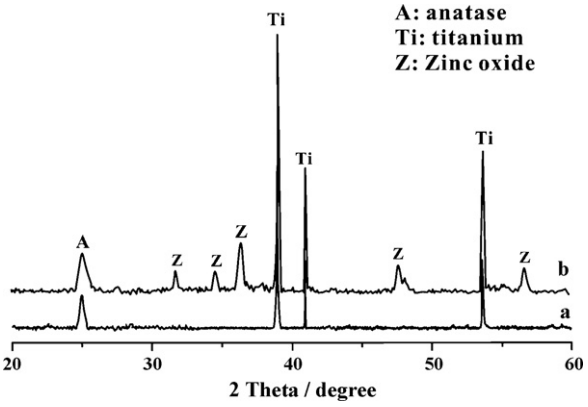

Fig. 3. XRD patterns of TiO_2 NTs and ZnO/TiO_2 NR/Ts samples.

K diffraction peaks of elemental Ti at 4.51 and 4.92 keV, the Kα diffraction peak of elemental O at 0.52 keV, and the diffraction peaks of 8.61 and 9.56 keV for Zn has appeared in this EDX analysis. The approximate ratio of Zn/Ti was estimated and the result indicated that the embedded amount of ZnO in the TiO_2 NTs is circa 9.41 wt%.

3.2. XRD analysis of ZnO/TiO_2 NR/Ts electrode

Fig. 3 shows the XRD patterns of TiO_2 NTs and ZnO/TiO_2 NR/Ts. The TiO_2 NTs demonstrate a regular anatase crystal structure, which is ascribed to the appearance of characteristic diffraction peaks at $2\theta = 25.3°$. In addition, ZnO/TiO_2 NR/Ts exhibits not only characteristic anatase diffraction peaks, but also other new XRD peaks at 31.9°, 34.6°, 36.4°, 47.7°, and 56.7°, which are ascribed to the hexagonal crystal system of ZnO.

3.3. Optical properties

Fig. 4 shows the UV–vis absorption spectra of TiO_2 NTs and ZnO/TiO_2 NR/Ts, which indicate the band gap absorption edges are around 372 and 410 nm, respectively. The relationship of the absorption coefficient and the incident photon energy of semiconductor are given by the following equation [37]:

$$\alpha(h\nu) \propto (h\nu - E_g)^n \quad (5)$$

where α is absorption coefficient, $h\nu$ is the energy of the incident photon, n is 0.5 and 2.0 for a direct transition semiconductor and indirect transition semiconductor, respectively. According to Eq. (5), the band gap energy of ZnO/TiO_2 NR/Ts is 3.03 eV and that of TiO_2 NTs is about 3.34 eV. The significant red shift of 0.31 eV may be owing to the high crystalline of ZnO and significant differences in the surface state, which promote the separate efficiency of photogenerated charges and extend the range of excited spectrum, and this finding is supported by data from other study [38].

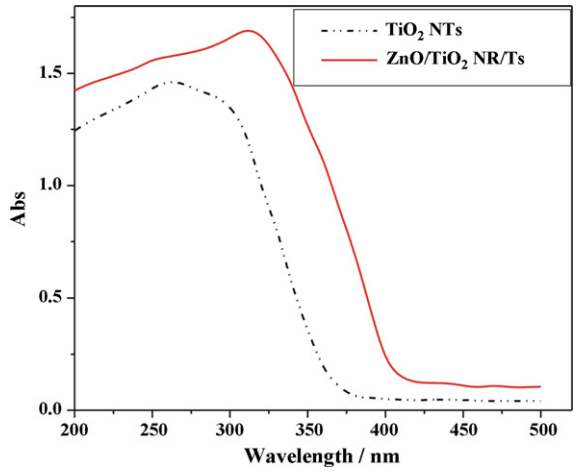

Fig. 4. UV–vis absorption spectra of TiO_2 NTs and ZnO/TiO_2 NR/Ts samples.

3.4. Photoelectrochemical properties

The photoelectrochemical performance of ZnO/TiO_2 NR/Ts is assessed using linear-sweep photovoltammetry, as shown in Fig. 5. The photovoltammetry can evaluate both the "dark" electrochemical behavior and the photoelectrochemical response in one experiment and under identical experimental conditions. The rise and fall of the photocurrent corresponded well to the illumination being switched on and off. The current response on both TiO_2 NTs and ZnO/TiO_2 NR/Ts in dark is insignificant even at a potential of up to 1.4 V, which means that no electrochemical oxidation occurred. Under illumination, a significant increase in the photocurrent is observed throughout the potential window. Moreover, the photocurrent is potential dependent. It increases as the applied potential is scanned toward more positive potential, particularly at potentials >0.1 V and this trend reaches a maximum photocurrent at a positive potential of 0.4 V. This indicates that the photogenerated electrons can be effectively driven by positive potential. The significant higher photocurrent density and the photocurrent onset shift to negative potentials on

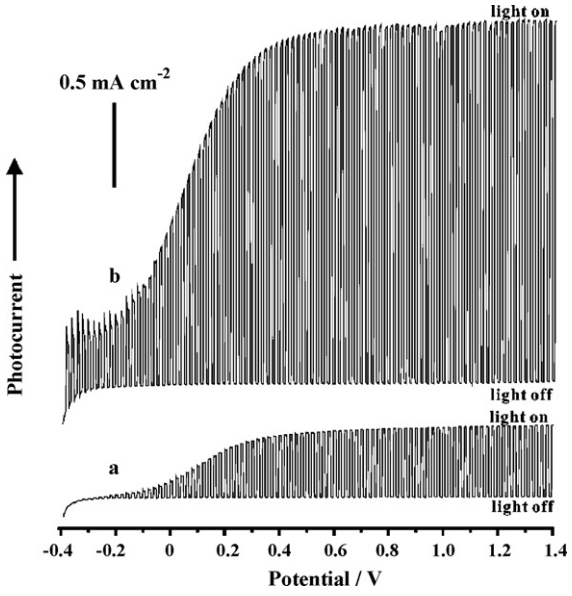

Fig. 5. Linear-sweep photovoltammograms with 0.1 Hz chopped irradiation of (a) TiO_2 NTs, and (b) ZnO/TiO_2 NR/Ts. Photovoltammograms were obtained at 2 mV/s using the full output of an 11 W UV lamp.

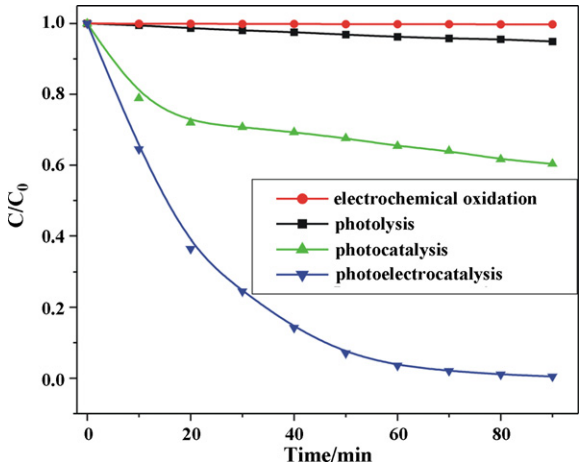

Fig. 6. Photoelectrocatalysis, photocatalysis, photolysis, and electrochemical oxidation processes of MO degradation using ZnO/TiO_2 NR/Ts electrode. Initial concentration of MO 5×10^{-5} M, applied potential 0.6 V.

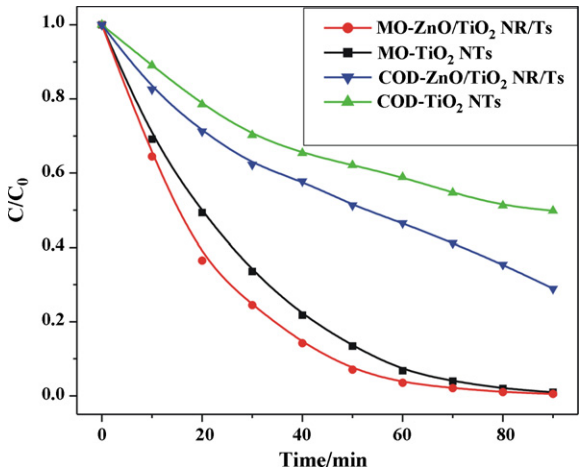

Fig. 7. The removal rate of MO and COD values by photoelectrocatalytic process on ZnO/TiO_2 NR/Ts electrode and TiO_2 NTs electrode. Same experimental conditions as those in Fig. 6.

ZnO/TiO_2 NR/Ts are due to the higher separate efficiency of photogenerated charges than that on TiO_2 NTs.

3.5. Photoelectrocatalytic degradation of MO on ZnO/TiO_2 NR/Ts electrode

To investigate the photoelectrocatalytic activity of ZnO/TiO_2 NR/Ts electrode, several photoelectrocatalytic experiments were carried out for MO degradation. The MO removal in the various degradation processes, that is, photoelectrocatalytic, photocatalytic, electrochemical oxidation, and direct photolysis processes, are presented in Fig. 6. It was obviously observed that the photoelectrocatalysis is the most powerful way to degrade the MO in aqueous solution. The complete removal of MO (99.5%) was observed after 90 min, while only 39.6% of the MO removal was obtained in photocatalytic process with the identical degradation time. The removal rate with direct photolysis was insignificant, which proved that the MO was stable with UV illumination. The result with electrochemical oxidation was also in good agreement with the data in Fig. 5, that is, the electrochemical oxidation did not occur evidently in this process.

The photoelectrocatalytic degradation of MO was performed using ZnO/TiO_2 NR/Ts electrode, and TiO_2 NTs electrode. The results were presented in Fig. 7. The removal rate of MO using ZnO/TiO_2 NR/Ts electrode was 85.8% after 40 min, while that using TiO_2 NTs was only 78.2% with the same time. After 90 min, the removal rates of MO on both ZnO/TiO_2 NR/Ts electrode and TiO_2 NTs were almost 100%. The removal rate could illustrate the degradation of MO. However, MO could not undergo complete degradation to produce CO_2 and H_2O, as a result, the intermediates were produced during the process. In order to show the mineralization rate of MO, COD removal was also investigated. As shown in Fig. 7, the removal rate of COD values on ZnO/TiO_2 NR/Ts electrode was 71.1% after 90 min, and that on TiO_2 NTs was 50.2% with the identical time, which meant that two of the electrodes were effective and the ZnO/TiO_2 NR/Ts electrode presented higher photoelectrocatalytic activity.

The Langmuir–Hinshelwood kinetic model formula has usually been applied to describe the photocatalytic and photoelectrocatalytic reactions. In this study, the experimental results can well fit the first-ordered reaction model equation, $\ln(C_0/C) = f(t) = kt$ (k is rate constant). The corresponding reaction rate constant k can be obtained from the degradation efficiency of MO. These reaction rate constants were ranked as ZnO/TiO_2 NR/Ts PEC ($k = 0.0591\ min^{-1}$) > TiO_2 NTs PEC ($k = 0.0515\ min^{-1}$) > ZnO/TiO_2 NR/Ts PC ($k = 0.0043\ min^{-1}$) > TiO_2 PC ($k = 0.0025\ min^{-1}$). Therefore, the superior photoelectrocatalytic activity of ZnO/TiO_2 NR/Ts is ascribed to the TiO_2 NTs configuration and the ZnO nanorods embedded modification in the tube channels. The ZnO/TiO_2 NR/Ts promotes the separation of photogenerated holes and electrons and improves the light energy harvest by expanding the excited spectrum range.

4. Conclusions

In this paper, the ZnO nanorods embedded in highly ordered TiO_2 nanotube arrays electrodes were first prepared via two electrochemical steps. The TiO_2 NTs electrode was fabricated by anodization method. The direct cathodic electrodepostion method was used to embed ZnO nanorods into TiO_2 nanotubes. The photoelectrochemical properties of ZnO/TiO_2 NR/Ts electrode were studied and the photocurrent was dramatically enhanced on the ZnO/TiO_2 NR/Ts electrode, compared with that on bare TiO_2 NTs electrode. The ZnO nanorods embedding modification can improve the photoelectrocatalytic activity of TiO_2 NTs. The TiO_2 NTs were used not only as photocatalytic semiconductor materials but also as template, which provided a general way to prepare novel hybrid nanomaterials.

Acknowledgements

The work is supported by the fund of Natural Science Foundation of PR China (No. 20327001 and 20675032) and Shanghai Rising-Star program (06QH14004).

References

[1] A. Fujishima, K. Honda, Electrochemical photolysis of water at a semiconductor electrode, Nature 238 (1972) 37–38.

[2] X.B. Chen, S.S. Mao, Titanium dioxide nanomaterials: synthesis, properties, modifications, and applications, Chem. Rev. 7 (2007) 2891–2959.

[3] M. O'Regan, M. Gratzel, A low-cost, high-efficiency solar cell based on dye-sensitized colloidal TiO_2 films, Nature 353 (1991) 737–740.

[4] Y. Shiraishi, N. Saito, T. Hirai, Adsorption-driven photocatalytic activity of mesoporous titanium dioxide, J. Am. Chem. Soc. 127 (2005) 12820–12822.

[5] A. Fujishima, T.N. Rao, D.A. Tryk, Titanium dioxide photocatalysis, J. Photochem. Photobiol. C 1 (2000) 1–21.

[6] Y.B. Xie, Photoelectrochemical reactivity of polyoxophosphotungstates embedded in titania tubules, Nanotechnology 17 (2006) 3340–3346.

[7] M. Hepel, I. Kumarihamy, C. Zhong, Nanoporous TiO_2-supported bimetallic catalysts for methanol oxidation in acidic media, Electrochem. Commun. 8 (2006) 1439–1444.

[8] H.Y. Zhu, Y. Lan, X.P. Gao, S.P. Ringer, Z.F. Zheng, D.Y. Song, J.C. Zhao, Phase transition between nanostructures of titanate and titanium dioxide via simple we-chemical reactions, J. Am. Chem. Soc. 127 (2005) 6730–6736.

[9] J.G. Yu, H.G. Yu, C.H. Ao, S.C. Lee, J.C. Yu, W.K. Ho, Preparation, characterization and photocatalytic activity of in situ Fe-doped TiO_2 thin films, Thin Solid Films 496 (2006) 273–280.

[10] M.H. Zhou, J.G. Yu, B. Cheng, Effects of Fe-doping on the photocatalytic activity of mesoporous TiO_2 powders prepared by an ultrasonic method, J. Hazard. Mater. 137 (2006) 1838–1847.

[11] H.G. Yu, J.G. Yu, B. Cheng, J. Lin, Synthesis, characterization and photocatalytic activity of mesoporous titania nanorod/titanate nanotube composites, J. Hazard. Mater. 147 (2007) 581–587.

[12] J.M. Macak, F. Schmidt-Stein, P. Schmuki, Efficient oxygen reduction on layers of ordered TiO_2 nanotubes loaded with Au nanoparticles, Electrochem. Commun. 9 (2007) 1783–1787.

[13] J.Q. Li, L.P. Li, L. Zheng, Y.Z. Xian, L.T. Jin, Photoelectrocatalytic degradation of rhodamine B using Ti/TiO_2 electrode prepared by laser calcination method, Electrochim. Acta 51 (2006) 4942–4949.

[14] B. Long, K. Nikitin, D. Fitzmaurice, Self-assembly of a tripodal pseudorotaxane on the surface of a titanium dioxide nanoparticle, J. Am. Chem. Soc. 125 (2003) 5152–5160.

[15] H. Sakai, T. Kanda, H. Shibata, T. Ohkubo, M. Abe, Preparation of highly dispersed core/shell-type titania nanocapsules containing a single Ag nanoparticle, J. Am. Chem. Soc. 128 (2006) 4944–4945.

[16] J.Q. Li, L. Zheng, L.P. Li, Y.Z. Xian, L.T. Jin, Fabrication of TiO_2/Ti electrode by laser-assisted anodic oxidation and its application on photoelectrocatalytic degradation of methylene blue, J. Hazard. Mater. 139 (2007) 72–78.

[17] J.M. Macak, M. Zlamal, J. Krysa, P. Schmuki, Self-organized TiO_2 nanotube layers as highly efficient photocatalysts, Small 3 (2007) 300–304.

[18] M. Paulose, K. Shankar, O.K. Varghese, G.K. Mor, B. Hardin, C.A. Grimes, Backside illuminated dye-sensitized solar cells based on titania nanotube array electrodes, Nanotechnology 17 (2006) 1446–1448.

[19] O.K. Varghese, D.W. Gong, M. Paulose, C.A. Grimes, E.C. Dickey, Crystallization and high-temperature structural stability of titanium oxide nanotube arrays, J. Mater. Res. 18 (2003) 156–165.

[20] Z.H. Zhang, Y. Yuan, G.Y. Shi, Y.J. Fang, L.H. Liang, H.C. Ding, L.T. Jin, Photoelectrocatalytic activity of highly ordered TiO_2 nanotube arrays electrode for azo dye degradation, Environ. Sci. Technol. 41 (2007) 6259–6263.

[21] G.K. Mor, K. Shankar, M. Paulose, O.K. Varghese, C.A. Grimes, Use of highly-ordered TiO_2 nanotube arrays in dye-sensitized solar cells, Nano Lett. 6 (2006) 215–218.

[22] J.H. Park, S. Kim, A.J. Bard, Novel carbon-doped TiO_2 nanotube arrays with high aspect ratios for efficient solar water splitting, Nano Lett. 6 (2006) 24–28.

[23] K. Zhu, N.R. Neale, A. Miedaner, A.J. Frank, Enhanced charge-collection efficiencies and light scattering in dye-sensitized solar cells using oriented TiO_2 nanotubes arrays, Nano Lett. 7 (2007) 69–74.

[24] X. Quan, S.G. Yang, X.L. Ruan, H.M. Zhao, Preparation of titania nanotubes and their environmental applications as electrode, Environ. Sci. Technol. 39 (2005) 3770–3775.

[25] S.P. Albu, A. Ghicov, J.M. Macak, R. Hahn, P. Schmuki, Self-organized, free-standing TiO_2 nanotube membrane for flow-through photocatalytic applications, Nano Lett. 7 (2007) 1286–1289.

[26] S.K. Mohapatra, M. Misra, V.K. Mahajan, K.S. Raja, Design of a highly efficient photoelectrolytic cell for hydrogen generation by water splitting: application of $TiO_{2-x}C_x$ nanotubes as a photoanode and Pt/TiO_2 nanotubes as a cathode, J. Phys. Chem. C 111 (2007) 8677–8685.

[27] C.H. Ye, Y. Bando, G.Z. Shen, D. Golberg, Thickness-dependent photocatalytic performance of ZnO nanoplatelets, J. Phys. Chem. B 110 (2006) 15146–15151.

[28] O.A. Fouad, A.A. Iamail, Z.I. Zaki, R.M. Mohamed, Zinc oxide thin films prepared by thermal evaporation deposition and its photocatalytic activity, Appl. Catal. B 62 (2006) 144–149.

[29] P. Suri, R.M. Mehra, Effect of electrolytes on the photovoltaic performance of a hybrid dye sensitized ZnO solar cell, Sol. Energy Mater. Sol. Cells 91 (2007) 518–524.

[30] M.A. Hasnat, M.M. Uddin, A.J.F. Samed, S.S. Alam, S. Hossain, Adsorption and photocatalytic decolorization of a synthetic dye erythrosine on anatase TiO_2 and ZnO surfaces, J. Hazard. Mater. 147 (2007) 471–477.

[31] D.C. Olson, J. Piris, R.T. Collins, S.E. Shaheen, D.S. Ginley, Hybrid photovoltaic devices of polymer and ZnO nanofiber composites, Thin Solid Films 496 (2006) 26–29.

[32] P. Ravirajan, A.M. Peiro, M.K. Nazeeruddin, M. Graetzel, D.D.C. Bradley, J.R. Durrant, J. Nelson, Hybrid polymer/zinc oxide photovoltaic devices with vertically oriented ZnO nanorods and an amphiphilic molecular interface layer, J. Phys. Chem. B 110 (2006) 7635–7639.

[33] J.J. Sene, W.A. Zeltner, M.A. Anderson, Fundamental photoelectrocatalytic and electrophoretic mobility studies of TiO_2 and V-doped TiO_2 thin-film electrode materials, J. Phys. Chem. B 107 (2003) 1597–1603.

[34] H.G. Yu, J.G. Yu, S.W. Liu, S. Mann, Template-free hydrothermal synthesis of CuO/Cu_2O composite hollow microspheres, Chem. Mater. 19 (2007) 4327–4334.

[35] J.G. Yu, H.G. Yu, B. Cheng, X.J. Zhao, J.C. Yu, W.K. Ho, The effect of calcinations temperature on the surface microstructure and photocatalytic activity of TiO_2 thin films prepared by liquid phase deposition, J. Phys. Chem. B 107 (2003) 13871–13879.

[36] H.J. Zhao, D.L. Jiang, S.Q. Zhang, K. Catterall, R. John, Development of a direct photoelectrochemical method for determination of chemical oxygen demand, Anal. Chem. 76 (2004) 155–160.

[37] H.M. Jia, H. Yan, Y.W. Tang, L.Z. Zhang, Synthesis and photoelectrochemical behavior of nanocrystalline CdS film electrode, Electrochem. Commun. 8 (2006) 1381–1385.

[38] R.S. Mane, W.J. Lee, H.M. Pathan, S.H. Han, Nanocrystalline TiO_2/ZnO thin films: fabrication and application to dye-sensitized solar cells, J. Phys. Chem. B 109 (2005) 24254–24259.